Drug screening and genome editing in human pancreatic cancer organoids identifies drug-gene interactions and candidates for off-label treatment

Christian K. Hirt[1,2], Tijmen H. Booij[3], Linda Grob[3,4], Patrik Simmler[1,2], Nora C. Toussaint[3,4], David Keller[3], Doreen Taube[1], Vanessa Ludwig[1], Alexander Goryachkin[1], Chantal Pauli[5], Daniela Lenggenhager[5], Daniel J. Stekhoven[3,4], Christian U. Stirnimann[3], Katharina Endhardt[5], Femke Ringnalda[1], Lukas Villiger[1,2], Alexander Siebenhüner[6], Sofia Karkampouna[7,8], Marta De Menna[7,8], Janette Beshay[9], Hagen Klett[9], Marianna Kruithof-de Julio[7,8], Julia Schüler[9], Gerald Schwank[1,2,*]

[1]Institute of Molecular Health Sciences, ETH Zurich, Switzerland

[2]Institute of Pharmacology and Toxicology, University Zurich, Switzerland

[3]NEXUS Personalized Health Technologies, ETH Zurich, Switzerland

[4]SIB Swiss Institute of Bioinformatics, Zurich, Switzerland

[5]Department of Pathology and Molecular Pathology, University Hospital Zurich, Switzerland

[6]Comprehensive Cancer Center, University Hospital Zurich, Switzerland

[7]Department for BioMedical Research, Urology Research laboratory, University Bern, Switzerland

[8]Department of Urology, Inselspital, Bern University Hospital, Switzerland

[9]Discovery Services, Oncotest, Charles River, Freiburg, Germany

Abstract

Pancreatic cancer (PDAC) is a highly aggressive malignancy for which the identification of novel therapies is urgently needed. Here, we establish a human PDAC organoid biobank from 31 genetically distinct lines, covering a representative range of tumor subtypes, and demonstrate that these reflect the molecular and phenotypic heterogeneity of primary PDAC tissue. We use CRISPR-Cas9 genome editing and drug screening to characterize drug-gene interactions with *ARID1A* and *BRCA2*. We find that missense- but not frameshift mutations in the PDAC driver gene *ARID1A* are associated with increased sensitivity to the kinase inhibitors dasatinib (p < 0.0001) and VE-821 (p < 0.0001). We conduct an automated drug-repurposing screen with 1,172 FDA-approved compounds, identifying 26 compounds that effectively kill PDAC organoids, including 19 chemotherapy drugs currently approved for other cancer types. We validate the activity of these compounds *in vitro* and *in vivo*. The *in vivo* validated hits include emetine and ouabain, compounds which are approved for non-cancer indications and which perturb the ability of PDAC organoids to respond to hypoxia. Our study provides proof-of-concept for advancing precision oncology and identifying candidates for drug repurposing via genome editing and drug screening in tumor organoid biobanks.

Keywords

Introduction

Pancreatic ductal adenocarcinoma (PDAC) is the most common tumor in the pancreas, and with a 5-year survival rate of <10% it is one of the deadliest of all cancers [1]. While recent successes in preclinical- and clinical research on pancreatic cancer have already led to a better understanding of the molecular causes of PDAC formation and progression, so far these findings have not been translated into successful novel therapies. Surgical resection has therefore remained the only curative therapy for PDAC [2]. However, most patients are diagnosed at an advanced disease state and are thus not eligible for surgery. Furthermore, in more than 80% of patients who undergo surgery the resected tumors recur within five years [3].

Pharmacological treatment of PDAC is mainly based on the combination chemotherapy regimens FOLFIRINOX (folinic acid, 5-FU, irinotecan and oxaliplatin) [4] or Gem-Abraxane (Gemcitabine, nab-paclitaxel) [5–7]. However, response to both of these chemotherapy regimens is relatively poor, with rapid development of resistances in the majority of patients [8]. More recently, several clinical trials have investigated the benefit of molecularly targeted drugs against pancreatic cancer, but so far only the EGFR inhibitor erlotinib has shown a moderate benefit in overall survival [9]. Taken together, there is an urgent need for more effective drugs to treat PDAC.

In the past, the majority of drug studies for PDAC were either based on 2D cancer cell lines or on patient-derived xenografts (PDX). Both models, however, have considerable drawbacks. While cancer cell lines reflect a subset of aggressive tumor cells that are

amenable to growth in 2D and only poorly represent the natural heterogeneity and phenotypes of primary cancers [10,11], *in vivo* PDX models are labor intensive and the number of drugs and drug-combinations that can be tested in these systems are limited [12]. More recently, protocols have been established to grow PDAC tissue as 3D organoids, which have the potential to bridge the gap between 2D cancer cell lines and PDX models [13,14]. Pancreatic organoids can be established from malignant cancers, and they closely reflect the phenotypic heterogeneity of the primary tumors [13,15]. Several recent studies, moreover, demonstrated strong correlations between drug responses in cancer organoids and patients [16–20]. When grown in multi-well tissue culture plates organoids are also amenable to high-throughput preclinical drug testing [16,17,28,20–27], although to the best of our knowledge large-scale drug screens in primary tumor organoids with > 350 compounds have not been reported yet.

In this study, we established a PDAC organoid biobank of 31 genetically distinct lines, which reflect that heterogeneity of PDAC and cover a range of tumor subtypes. In order to enable screening of a larger number of compounds, we developed an automated screening pipeline employing an integrated robotic screening platform for culturing, drug delivery and viability analysis. We tested for drug-gene interactions with *ARID1A* and BRCA2 and conducted a drug repurposing screen to discover effective compounds from a library of 1,172 FDA-approved drugs. We identified 26 compounds that showed effective activity in inhibiting growth of PDAC organoid lines, and validated the growth inhibitory activity of these compounds *in vitro* and *in vivo*. Our study demonstrates the effectiveness of using a genetically diverse organoid biobank to systematically screen a large compound set and identify candidates for drug development and repurposing.

Results

Establishment of a human PDAC organoid biobank that recapitulates the phenotypic and genomic heterogeneity observed in patients

In order to generate an organoid biobank for pancreatic cancer, we established PDAC organoid lines from surgically resected specimens and from patient tumor tissue that was initially expanded in PDX models (11 and 20 lines, respectively). In addition, we established healthy, i.e. non-cancerous pancreatic ductal organoid lines from surrounding tissue of resected PDAC specimens, and from pancreatic tissue obtained during pancreatic islet isolation (five and four lines, respectively). Procedures for organoid establishment were adapted from previously published protocols [14,15]. The efficiency of generating KRAS-mutant PDAC organoids was 65% from surgically resected primary tumor tissue, and 95% from PDX-expanded tumor tissue (Table S1). In line with previous studies, we observed high diversity in PDAC organoid phenotypes. These ranged from cystic hollow structures consisting of a single-layered epithelium with uniform nuclei, similar to healthy pancreas organoids, to dense multi-layered lobular tumor nodules with polymorphic nuclei, resembling anaplastic PDAC (Figure 1A). Importantly, organoid phenotypes correlated strongly with *in vivo* morphology of primary PDAC tumors in patients and xenografts (Figures 1A and S1A-B). More differentiated tumors with tubular and large ducts gave rise to organoids with a thin epithelial layer, and poorly differentiated tumors with a solid

growth pattern gave rise to lobular organoids with pleomorphic cells. Importantly, organoid phenotypes remained stable over multiple passages and after repeated subcutaneous transplantation into mice (Figure S1B, C).

In line with phenotypic heterogeneity we also observed differences in expression of the PDAC prognosis markers *TP53* and *SMAD4* [29] (Figure 1A), and differences in growth-factor dependency assays (Figure 1B); unlike healthy pancreatic organoids which require the signaling molecules Wnt, R-spondin, Noggin, EGF, and the TGF-beta inhibitor A83-01 for growth, PDAC organoids grew largely independent of these factors. Of the 14 tested PDAC lines, 12 could be expanded without Wnt or EGF, 11 lines could be expanded without Noggin, five lines could be expanded without R-Spondin, and none of the lines required the TGF-beta inhibitor A83-01 for growth (>6 passages tested).

Several recent studies have used analysis of gene expression using bulk RNA-seq to classify PDAC into different molecular subtypes [30–34]. When we performed RNA-seq on five PDAC organoid lines and applied the high tumor cellularity classification system [32], we found two lines associated with the classical subtype, one line associated with the basal-like subtype, and two lines of an intermediary phenotype (Figure 1C). Together these results confirm that the heterogeneity of primary PDAC samples is retained in PDAC organoids, and suggest that our biobank covers a range of different tumor subtypes.

To next assess if our biobank reflects the expected mutational spectrum that is observed in PDAC patients [30–34], we analyzed 25 samples from our biobank using NGS (Figure 1D, Table S4). Given that we did not receive matched normal tissue for all PDAC samples, we select against germline variants by excluding known human polymorphisms and filtering for SNVs and InDels with high or moderate protein impact. As expected, frequencies of mutation in common PDAC tumor driver genes in our organoid biobank were similar to that found in previous studies based on sequencing PDAC patients. We detected mutations in all of the three most frequent PDAC driver genes (*KRAS*, *CDKN2A*, and *TP53*) in > 60% of our samples, core-components of the TGF-β/BMP in 80% of the samples (*ACVR1B*, *ACVR2A, SMAD4* and *TGFBR2*), and subunits of the SWI/SNF chromatin remodeling complex in 40% of the samples (*ARID1A, ARID2, PBRM1* and *SMARCA4*). Similar to previous PDAC studies we also observed a tendency of mutual exclusivity for mutations in *KRAS* and *BRAF*, for mutations in the SWI/SNF subunits, and for mutations in the TGF-β/BMP pathway genes.

Drug sensitivities in PDAC organoids differ from monolayer cultures and correlate with xenograft models

To enable high-throughput compound screening in our PDAC organoid lines we established a fully automated drug screening platform. Confirming previous studies, we found that organoid growth and drug responses were similar in liquid-overlay culture systems and standard Matrigel domes (Figure S2A and S6). The liquid-overlay culture system, however, is more scalable to screen a larger number of compounds, and we therefore continued to use this screening system in our study. In our optimized protocol we seed dissociated organoids on wells with Matrigel-supplemented media, expand them for six days in the presence of drugs, and perform growth and viability analysis using the CellTiterGlo®3D assay (Figure

2A, S2B-C). To first test if drug responses differ between organoids and conventional 2D cancer cell lines, we generated monolayer cell cultures from two PDAC organoid lines of our biobank, and treated the cultures with a panel of 40 drugs that were either approved by the FDA or in clinical trials for PDAC (Figure S2D, Table S6). Confirming that the culture environment has a strong influence on drug responses, and supporting our assumption that drug screening in organoids could lead to the identification of a different set of compounds compared to previous 2D drug screens, we found that response profiles clustered by culture condition (2D vs. 3D) rather than the genetic background (Figure 2B).

We next assessed whether drug responses in 3D organoids are predictive for *in vivo* drug responses, and compared the efficacy of the EGF-inhibitor erlotinib in seven PDAC samples grown as organoids and PDX models. As expected from clinical studies in PDAC patients [9], we observed high variability in erlotinib response between the different PDAC samples (Figure 2C, 2D). However, a strong correlation was observed within isogenic PDAC lines treated *in vitro* and *in vivo* (p<0.05, Spearman's rho=-0.78) (Figure 2E). These results are in line with previous studies, which suggest that drug responses in organoids are predictive for *in vivo* efficacy in xenograft models and patients [16,17,27,18–21,23–26]. Notably, we also attempted to systematically test erlotinib responses in isogenic 2D monolayer cell lines, but were only able to establish lines from three of the seven PDAC samples. Nevertheless, within this small dataset 2D cell lines were less accurate in predicting *in vivo* erlotinib responses compared to 3D organoids (Figure S2E).

Mapping drug-gene interactions in PDAC-organoids

Interactions with approved drugs have been reported for some of the genes reported to be recurrently mutated in PDAC. *ARID1A* encodes for a subunit of the SWI/SNF chromatin remodeling complex, and is frequently mutated in ovarian clear cell carcinomas where it displays a synthetic lethal interaction with the tyrosine kinase inhibitor dasatinib and the ATR-inhibitor VE-821 [35,36]. To assess if mutations in *ARID1A* also lead to higher sensitivity to dasatinib and VE-821 in PDAC, we compared the efficacy of both drugs in PDAC organoid lines either wildtype (WT) or mutant for *ARID1A* (Figure 3A). We tested three lines WT for *ARID1A*, two lines with frameshift mutations where protein expression was absent, and three lines with missense mutations where protein expression was preserved (Fig. 3B). Interestingly, we observed higher sensitivity for both drugs in PDAC organoid lines with missense mutations, but not in PDAC organoid lines with frameshift mutations, suggesting that the drug-gene interaction requires expression of malfunctional ARID1A protein (Figure 3C). To further investigate this hypothesis, we used CRIPSR-Cas9 to engineer frameshift mutations in exon 1 of *ARID1A* (Figure 3C, D). In line with our hypothesis, we did not observe an increase in drug sensitivity in the lines that were initially WT for *ARID1A*, but a significant decrease in sensitivity in the three organoid lines that initially harbored a missense mutation in *ARID1A* (Figure 3D, E). Taken together, these results suggest that in PDAC drug-gene interactions for *ARID1A* with dasatinib and VE-821 are limited to missense mutations where expression of malfunctioning ARID1A is preserved.

BRCA2 encodes for a protein involved in DNA double-strand break repair, and its inactivation leads to homologous recombination deficient (HRD) tumors [37]. *BRCA2* is frequently mutated in PDAC, as well as ovarian- and breast cancer where it displays a synthetic lethal interaction with PARP inhibitors (PARPi) [38,39]. Recent clinical studies suggest that also PDAC patients with *BRCA* mutations might profit from PARPi therapy [40], prompting us to assess the responsiveness of PDAC organoids with- and without *BRCA* mutations to PARP inhibitors. We selected three lines WT for *BRCA*, three lines with germline or somatic mutations in *BRCA2*, and in addition used CRISPR/Cas9 to engineer two knock-out lines with loss in *BRCA2* gene expression (Figure S3 A, B). When we first treated organoids with oxaliplatin, a platinum-based compound that showed higher activity in patients with germline BRCA mutations [41], we observed a slight trend towards increased sensitivity in *BRCA2* mutant lines (Figure S3 C). However, when we next treated organoid lines with PARP inhibitors veliparib, olaparib and talazoparib, no significant differences in drug response based on the *BRCA2* mutational status were found (Figure S3 C). These results might be explained with HR deficiency in BRCA WT PDAC organoids, since analysis of COSMIC mutational signatures also showed high levels of HRD-related signature 3 in these tumors (Figure S3 D). Notably, these findings are in line with recent clinical studies, which suggest that a substantial proportion of *BRCA* WT patients could benefit from PARPi therapies [38].

Fully automated high-throughput drug screening in organoids identifies new off-label compounds

Previously published drug screens in organoids have been performed with small- to medium-sized compound libraries [16,17,20,21,23–26,28]. To be able to screen a larger set of compounds, we developed a fully automated organoid screening pipeline in which an integrated robotic screening platform combines automated organoid culturing, drug delivery, and viability analysis (Figure 4A). Using this approach, we performed a drug-repurposing screen with a library covering 1,172 drugs approved by the FDA for a variety of different medical indications, including cancer, infection, inflammation, cardiovascular diseases, or neurological disorders (Figure 4B). We screened two different organoid clones of one PDAC sample with a single dose of 1μM. This concentration was chosen as in commercial PDAC cell lines the IC50 value of FDA approved drugs is commonly between 1-10μM (Figure S4A, B). Confirming the high quality of our screening assay, we obtained Z-prime (Z') factors above 0.5 for 7 out of 8 screened plates, with the remaining plate having a Z'-factor of 0.47 (Figure 4C and Figure S4C, D). Using a threshold of 0.5 for the effect size (ES) and 0.01 for the FDR we identified 26 hit compounds (Figure 4D, Table S7). Within the list of effective drugs were the standard PDAC chemotherapy compounds paclitaxel and gemcitabine but not 5-FU, which in PDAC organoids is only active at higher doses (Figure S5A). 19 of the hits were chemotherapy drugs currently approved for other cancer types, including pyrimidine-analogs as well as microtubule-, telomerase-, topoisomerase-, and proteasome- inhibitors. Five of the hits were compounds currently not approved as anti-cancer drugs; the cardiac glycoside ouabain, the anti-protozoal drug emetine, the antiseptic drug cetylpyridinium chloride, and the anthelmintic drugs flubendazole and oxibendazole.

Ex vivo and in vivo validation of screening hits

To validate our screening hits, we tested the 26 identified hits on a panel of ten human PDAC organoid lines, four healthy pancreatic organoid lines, three PDAC monolayer cell lines derived from PDAC organoids, and two commercially available PDAC monolayer cell lines (ASPC-1, PANC-1). While 22 of the 26 compounds were potent in the majority of PDAC organoid lines, most compounds were not active in 2D cancer cell lines (effect size <0.5; Figure 5A and S5B, C). Further verifying our hits, we observed similar drug responses when PDAC organoids were grown in classical 3D drop culture systems (rho-values of 0.65-0.89 - Figure S6A-C). In addition, a subset of hits was also effective in killing PDAC organoids derived from metastatic liver lesions (Figure S6D, E), suggesting that these compounds also have potential for treating PDAC metastases.

Since organoids can also be established from healthy pancreatic ducts, we next assessed if our hits show different efficacy in PDAC organoids compared WT organoids. Hierarchical clustering and correlation analysis, however, did not lead to a clear separation of both groups (Figure 5B), and only for the topoisomerase inhibitors topotecan, epirubicin, mitoxantrone and teniposide higher potency was observed in PDAC lines (Figure 5A). These results were expected, since WT organoids continuously proliferate and do not resemble healthy pancreatic tissue; differences in drug responses would therefore only be expected for compounds targeting cancer specific vulnerabilities independent of cell proliferation.

We next grouped the 22 hits according to their mechanisms of action, and chose one compound per group (8 drugs) for *in vivo* analysis. By generating *in vitro* dose-response curves and taking in consideration LD50 doses (Figure S5C and Table S7), we designed individual drug administration plans for the treatment of xenograft models. The PC02 PDAC line was subcutaneously transplanted, and once tumors reached a size of 100mm^3, mice were treated with compounds or control vehicles over 21 days (Figure 5C-D). While the most effective compound tested was the standard PDAC drug gemcitabine, leading to a 95% reduction in tumor volume compared to control vehicle (p < 0.001), also five other drugs showed a significant reduction in tumor volume (Carfilzomib -67.7%, p = 0.02; Ouabain -58.5%, p = 0.001; Doxorubicin -57.9%, p = 0.011; Emetine -54.3%, p = 0.01; Vinblastine Sulfate -54%, p = 0.028). These data suggest that validated hits from the drug-repurposing screen might be promising candidates for second line therapies in PDAC patients that developed resistances to standard chemotherapy drugs.

Emetine and ouabain attenuate HIF-1α response in PDAC organoids

Although emetine and ouabain are currently not approved for cancer treatment, both compounds have recently shown to be effective against chronic lymphocytic leukemia by targeting hypoxia inducible factor (HIF)-1α activity [42]. Hypoxia is also a characteristic feature of advanced PDAC [43] (Figure 7A), and is associated with reduced overall survival (Figure 6B), prompting us to investigate whether emetine and ouabain target PDAC cells via attenuating HIF-1α activity. We first assessed if the hypoxic state of *in vivo* PDAC tissues is conserved in organoid cultures, and compared HIF-1α target gene expression in two isogenic PDAC lines grown as PDX, organoids, or 2D monolayers. Under normoxic conditions (21% O$_2$ atmosphere), *CAIX* and *VEGFA* were indeed significantly higher

expressed in PDAC organoids compared to classical monolayer cells (Figure 6C). In line with these results, treatment with BAY-87, a known inhibitor of hypoxia-induced gene activation, specifically blocked growth in 3D PDAC organoid cultures but not in the corresponding 2D cell lines (Figure S7A). Importantly, when we compared the efficacy of emetine and ouabain between PDAC organoids and 2D monolayer cell lines we found that both compounds behaved similar to BAY-87, and more effectively blocked cell growth in PDAC organoids compared to monolayer cell lines (Figure 5A). In addition, they led to a significant downregulation of HIF-1α target gene expression 24h after drug treatment (Figure 6D). Together, these results support the hypothesis that emetine and ouabain inhibit PDAC organoid growth by interfering with their ability to adapt to hypoxia.

Discussion

2D cancer cell lines have been excessively used as *in vitro* models for PDAC. However, while these classical monolayer cell lines are amenable for high-throughput screening, the success rate in establishing 2D cancer cell lines from patients is extremely low [44,45], they poorly reflect heterogeneity of the primary PDAC tissue [13], and have limited potential in predicting drug efficacy [46]. While a valuable alternative to cancer cell lines are PDX models, they are extremely cost intensive and therefore not suitable for high-throughput drug screening. In our study we established a biobank of >30 genetically distinct human PDAC organoid lines. We show that PDAC organoids correlate with the molecular and phenotypic heterogeneity observed in primary PDAC tissue, as well as *in vivo* drug responses. These data are in line with several recent studies, which found good correlations in drug responses between organoids, xenograft models, and patients [17–20,27].

Since organoids are accessible to *in vitro* manipulations, we also applied drug screening in combination with CRISPR/Cas9 genome editing to study drug-gene interactions for frequently mutated PDAC driver genes. Analyzing *ARID1A*, we found that the positive correlation between mutations in *ARID1A* and sensitivity to dasatinib and VE-821 – initially described in ovarian cancer - is conserved in PDAC. However, our results also suggest that this drug-gene interaction is critically dependent on the type of mutation; only PDAC organoid lines with missense mutations in *ARID1A*, but not with nonsense or frameshift mutations showed increased drug sensitivity. Based on these results, we speculate that identification of patients with response to targeted drugs could be significantly improved if the type of mutations and not simply the presence or absence of mutations in tumor suppressor genes would be taken into account. The latter is currently the standard in umbrella trials [47].

Unlike previous organoid screening studies that focused on small- to medium scale drug panels [16,17,28,20–27], we used a fully automated screening platform to perform a drug-repurposing study covering 1,172 FDA-approved drugs. Within the *in vivo* validated hits were several drugs that are currently only approved for non-cancer indications. These include emetine and ouabain, for which we could show that they specifically kill PDAC organoids by interfering with their ability to respond to hypoxia. Interestingly, when we treated 2D PDAC cell lines grown under hypoxia with emetine, ouabain, or BAY-87, we observed suppression of HIF-1a reporter activity but no increase in cell death (Figure

S7C-E). Performing the drug screen in 3D organoids was therefore essential for identifying these compounds as hits. Emetine has already been tested in phase I and II clinical trials for different solid tumors [48–50]. Although these trials were discontinued due to its very narrow therapeutic index, recent preclinical studies suggest that in combination with other compounds emetine might be effective against bladder and ovarian cancer at lower doses [51,52]. In our study, we observed efficacy for PDAC in a PDX mouse model with a dose of 2mg/kg/d. This is equivalent to 0.16mg/kg in humans based on allometric scaling [53], and corresponds to approximately 16% of the standard dose given to patients. Ouabain is a Na^+/K^+-ATPase inhibitor, which has recently been shown to alter the invasive potential of breast cancer cell lines [54]. In addition, ouabain dissociates circulating breast cancer cell clusters, leading to reduced metastasis formation [55]. We found that a dose of 0.56mg/kg/d significantly reduced growth of PDAC xenografts in mice. Notably, it is difficult to translate results from murine xenograft studies with ouabain to humans, due to its toxicity in human cells at lower doses than in rodent cells [56]. However, the dose used in mice was equivalent to the human dose of 0.046mg/kg, which corresponds to approximately 54% of the dose administered to healthy volunteers in a clinical study [53,57].

Limitations of the study

Certain limitations of our study should be noted. First, PDAC organoids are only comprised of cancer cells and do not include the complex tumor microenvironment. This might lead to significant differences between *in vitro* and *in vivo* drug responses. The establishment of more advanced organoid models, where tumor cells are co-cultured with the stromal component and immune cell populations, would likely improve predictions for drug responses in patients. Second, our PDAC organoid biobank was limited to 31 patient samples, and less common PDAC driver genes were therefore only mutated in a few organoid lines. This prevented us from systematically correlating drug responses to a larger set of PDAC driver mutations. In the future, the establishment of more extensive cancer organoid biobanks could circumvent this restraint. Third, limitations in resources prevented us from performing large-scale drug screening with different drug concentrations, and our screen was only conducted with a single compound concentration of 1μM. Thus, some compounds with a higher IC50 might have been missed, while others with a lower IC50 might be false positive hits due to toxicity at the screened concentration. Since the majority of expenses for drug screening were caused by the use of Matrigel for organoid growth, the development of synthetic hydrogels that could be readily produced on a large scale would significantly reduce costs, and facilitate the use of multiple compound concentrations in high-throughput drug screening.

In conclusion, we established a heterogenous human PDAC organoid biobank that covers different tumor subtypes. By utilizing the genetic diversity of organoid lines and genome editing we were able to analyze drug-gene interactions, which revealed an association between missense mutations in *ARID1A* and increased sensitivity to dasatinib and VE-821. Moreover, high-throughput drug screening with a panel of 1,172 FDA-approved drugs identified several compounds that effectively kill PDAC cells *in vitro* in organoid cultures and *in vivo* in PDX models. In the future, it would be interesting to test whether these compounds could be applied as second line treatments in PDAC patients that developed

resistance to standard therapies. In addition, our approaches for high-throughput compound screening and for testing drug-gene interactions could also be applied in organoid biobanks of other tumor types, facilitating the development of targeted and personalized treatments in multiple cancer entities.

Method details

Human pancreatic organoid line culture

Human pancreatic tissue was provided by the Department of Pathology and Molecular Pathology, University Hospital Zurich, based on informed consent and study approval from the ethical committee (BASEC-Nr. 2017-01319). To establish PDAC organoid lines, tissue was chopped and digested for 30 min (WT tissue) and 4-12 hours (tumor tissue) in full medium containing collagenase type II (5 mg/ml). The digestion was stopped with advanced DMEM/F12 medium. Cells were seeded as 20µl drops of Matrigel (Corning, growth factor reduced) into a 48-well suspension culture plate. PDX tumor tissues were provided by Charles River Research Services, Germany. PDX-PDAC organoid lines were established from frozen PDX cell suspensions. After defreezing 100'000 PDX cells were pre-cultured for 4h on 24 well cell culture plates in organoid medium before matrigel embedding to reduce the amount of murine stromal cells. Afterwards, the standard organoid culture protocol was followed. To establish healthy pancreas organoid lines derived from islet transplant programs, ductal cells were hand-picked to assure that no islets would be subcultured, followed by a mechanical dissociation prior to embedding in matrigel drops. Pancreas and human PDAC organoids were cultured in Advanced DMEM supplemented with 10×10^{-3} M HEPES, 1x Glutamax, 1% Penicillin/Streptomycin, 1x B27, 1.25×10^{-3} M N-acetylcysteine, 50% Wnt3a CM (Conditioned Medium), 10% R-spondin-1 CM, 10% noggin CM, 10×10^{-3} M nicotinamide, 1×10^{-6} M prostaglandin E2, 50 ng mL^{-1} EGF, 10×10^{-9} M gastrin, 100 ng mL^{-1} FGF10 and 0.5×10^{-6} M A83-01.

sgRNA design and lentivirus production

sgRNAs were cloned into the lentiCRISPR v2-Blast vector (Addgene #83480). Three sgRNAs per gene were designed. For BRCA2 exon 11 was targeted and for ARID1A exon 1 was targeted within a 250 bp region (Star Methods Table). sgRNAs were cloned into the vector using *BsmBI* digest. Lentiviral particles were produced by transient transfection of HEK293T cells with sgRNA vectors along with the packing constructs PAX2 and VSV-G. Virus-containing supernatants were harvested on Day 4-5 after transfection and passed through a 0.45um filter. Viral supernatant was ultra-centrifuged at 10'500 rpm for 2h and afterwards stored at -80°C.

Transduction of organoid lines

Organoids from matrigel drops were washed with ice-cold PBS and the pellet resuspended in TripLE for 7min at 37°C to obtain single cells. After trypsinization, cells were resuspended in 500µl of growth medium containing the Rho kinase inhibitor Y-27632, 4µg/ml of Polybrene and 20µl of the concentrated lentivirus. The cell suspension was plated in 48 well plates at high density and centrifuged at 600g at 32°C for 60min, followed by an incubation at 37°C for 2-4h. Cells were then collected in Eppendorf tubes, centrifuged

at 1000g, resuspended in ice-cold matrigel and plated in 20μl drops in a 48-well plate. Two days after transduction, 5μg/ml blasticidin was added to the medium. Single organoids were picked and expanded to obtain clonal organoid lines which were characterized by western blotting and next generation sequencing.

Histological staining

Organoids were encapsulated in 100μl heat-inactivated human plasma (Transfusionsmedizin, Zurich) and 5μl thrombin (50 U/ml). The embedded tissue was then fixed overnight in 4% paraformaldehyde at 4°C and paraffin embedded. Subsequently, sections (5 μm) were deparaffinized, hydrated, and stained with hematoxylin and eosin (H&E). Immunohistochemistry for p53 and SMAD4 was performed after antigen retrieval at the Department of Pathology and Molecular Pathology of the University Hospital Zurich.

Growth factor dependency test

Organoid line growth factor dependency was tested in biological duplicates in classical organoid culture over 6 passages. Medium without the representative growth factor was refreshed twice per week. Representative images were obtained by Brightfield-Imaging and compared to standard-medium condition, prior to splitting. Organoid lines were split in a 1:2 ratio every 7-14 days, depending on the individual growth rate.

Next generation sequencing and analysis (Analysis for each sample: Table S1)

Sample preparations—DNA/RNA was either processed directly from freshly established tumor organoid lines (fresh PDAC-derived organoid lines) or from tumor xenograft cell suspensions (PDX-derived organoid lines). Either a phenol-chloroform or a column-based DNA-extraction (DNesay Blood and Tissue Kit, Qiagen) was performed. For RNA isolation a column-based extraction was performed (RNeasy Kit, Qiagen).

Whole exome sequencing and mutation calling (Overview for each sample: Table S3)

PDAC organoids established from Surgical Specimens: Agilent Sure Select Human All Exon v6+UTR kits were utilized to build the sequencing libraries. DNA of tumor was then subjected to paired-end (152 bp) whole-exome sequencing (WES) using the Illumina NovaSeq platform. Tumor and matched wild type WES data was analyzed based on the framework described in (Singer et al. 2018). Adapters were trimmed using SeqPurge (v.0.1-438-g79b1e8b) (Sturm et al. 2016). The sequence reads were aligned to the human genome (hg38) using BWA mem (v.0.7.12-r1039). Post-processing of the mapping was done using Picard MarkDuplicates (v.2.18.17), BamClipOverlap (v.2018_11), and GATK IndelRealigner (v.3.8). A combination of three variant callers was used to call somatic variants (SNVs and InDels), namely MuTect (v.1.1.4) for SNVs, as well as VarScan2 (v.2.4.3) and Strelka (v.1.0.14) for both SNVs and small InDels. Only SNVs and InDels reported by at least two callers were considered in the subsequent analyses in order to identify variants with greater confidence and reduce the number of false positive calls. The detected variants were annotated using SnpEff and SnpSift (v.4.3t) as well as dbNSFP

(v2.9). SNVs with variant allele frequencies of 0.8 or more are considered homozygous. All other SNVs are considered heterozygous.

PDAC organoids established from PDX cell suspensions: Exonic regions were targeted using one of the following Agilent SureSelect Human All Exon kits, V1 38 MB/ V4 51 MB/ V5 50 MB/V6 60 MB, and sequenced with Illumina HiSeq-2000/2500 (100bp or 126bp paired-end). The sequence reads were independently aligned to the human genome (hg38) and the mouse genome (mm10) using BWA mem with default parameters. Reads with a better BWA mapping score to the mouse than the human genome were considered mouse stroma and removed from the human alignment using PicardTools (http://broadinstitute.github.io/picard/). Post-processing included duplicate removal, local indel realignment, and base recalibration using GATK. Three variant callers were used to call variants: GATK's UnifiedGenotyper, a combination of Samtools mpileup and bcftools caller, as well as Freebayes. Only variants identified by all three callers, with at least three supporting reads, and a minimum variant frequency of 0.05 were subsequently considered. These variants were annotated with SnpEff and further filtered by (1) selecting only single nucleotide variants (SNVs) as well as small insertions and deletions (InDels) with a high or moderate impact based on UCSC or Ensembl transcripts and (2) excluding known human polymorphisms found in Hapmap, CGI 69 genomes, EVS + 1000 genomes, or dbSNP. SNVs assigned a genotype of "1/1" by the somatic variant caller are considered homozygous. All other SNVs are considered heterozygous.

RNA sequencing—Sequencing libraries were prepared using the Illumina TruSeq RNA Sample Preparation Kit. The libraries were sequenced on one lane on a NovaSeq instrument with 151 bp paired end (PE) reads. Raw reads were first aligned with STAR v.2.5.3a. Quantification was then performed using htseq-count from the HTSeq package (v.0.9.1) with the intersection-nonempty option. In order to minimize differences between samples and to normalize with respect to library size the count-data has subsequently been transformed and scaled using the rlog function from DeSeq2 and standardized to mean 0 and variance 1. Afterwards, the profiles were assigned to tumor subtypes according to their similarity (Spearman correlation) with previously published reference profiles. To reduce any systematic difference between the two data sets the reference profiles have been normalized and standardized as well.

DNA copy number variation analysis

PDAC organoids established from Surgical Specimens: Low-coverage whole genome sequencing: DNA was subjected to paired-end (152 bp) whole genome llumina sequencing. Adapters were trimmed using SeqPurge (v.0.1-438-g79b1e8b). The sequence reads were aligned to hg38 using BWA mem (v.0.7.12-r1039). Post-processing of the mapping was done using Picard MarkDuplicates (v.2.18.17) and GATK IndelRealigner (v.3.8). Copy-number variants (CNVs) were called using bicseq2 (v.0.2.4). Only CNVs called with a p-value less than or equal to 0.05 were considered in subsequent analyses.

PDAC organoids established from PDX cell suspensions: The Affymetrix Genome-Wide Human SNP Array 6.0 was used for the detection of copy number variation. PICNIC was

used to determine copy numbers for each segment. The segment files produced by PICNIC were transformed to gene counts based on the hg38 human reference genome coordinates. For genes located in more than 2 segments, the final copy number was determined by using in this order 1) homozygous deletion (PICNIC state: 0, 2) gene amplification (PICNIC states: 8-14), or 3) moderate copy number loss to moderate copy number gain (PICNIC states: 1-7, with 3-5 considered no change).

Mutation signatures—The relative contribution of COSMIC mutation signatures was obtained using the Mutational Signatures in Cancer (MuSiCa) web service (http://bioinfo.ciberehd.org:3838/MuSiCa/, accessed on August 20, 2021) [60] . MuSiCa is based on the R/Bioconductor package MutationalPatterns [61] to quantify the contribution of COSMIC signatures in a sample.

Real-time quantitative PCR

Total RNA was extracted from PDAC organoids using the RNeasy Mini Kit (Qiagen) and cDNA was synthesized using the GoScript Reverse Transcriptase System (Promega). Real-time qPCR was performed using the Fast SYBR Green PCR master Mix (Applied Biosystems) and the StepOnePlus Real-Time PCR System 96 or the Light Cycler System 384 (Roche). Either *ACTB* (BRCA2) or *TBP* (HIF-1α -target genes) was used as Housekeeping gene. Relative gene-expression levels were calculated using the delta-delta CT method. The primer sequences are listed in the methods table.

Western blot analysis

Cell lysates were prepared in RIPA buffer supplemented with a protease (cOmplete, Roche) and phosphatase inhibitor (PhosSTOP, Roche) cocktail. Protein concentration was measured by BCA protein assay (Pierce, Thermo Scientific). Equal amounts of protein were diluted in sample reducing reagent 10x (NuPage Invitrogen) and LDS Sample Buffer 4x (NuPage Invitrogen) for 10min at 55°C. Samples were loaded on 3-8% NuPage Tris-Acetate gradient gels run for 45min at 150 V and then transferred for 3.5h at 30V to an Amersham Protan NC Nitrocellulose membrane (0.2μm). Membranes were blocked for 1h at room temperature with 3% bovine serum albumin (BSA Fraction V, Roche). Incubation with primary antibody was done overnight at 4°C. The next day, the western blot was washed 3x10 min in TBS-T. The secondary antibody, diluted in 3% BSA-blocking buffer, was applied to the membrane and incubated for 1h at room temperature. After another three washes with TBS-T, detection of the signal was achieved by incubating the membrane with the Western Bright Quantum (Advansta). Signal detection was carried out using a Fusion Solo S. The following antibodies were used at the indicated dilution: anti-Actin (Cell Signaling #4970, 1:4'000), anti-BRCA2 (Merck OP95, 1:1'000), anti-ARID1A (Novusbio NBP1-88932, 1:5'000), anti-mouse IgG-HRP (Merck 401253, 1:5'000) and anti-rabbit IgG-HRP (Cell Signaling #7074P2, 1:5'000).

Chemical compounds

An FDA-approved compound library containing in total 1'172 FDA-approved drugs (L1300, Selleck Chemicals) was purchased as 100μl 10mM DMSO stock and sealed under argon gas to prevent deterioration using a thermal sealer (Agilent PlateLoc). Hit molecules that

were selected after screening the FDA-approved compound library as described below were re-ordered through SelleckChemicals and provided as 10mM stock solutions in DMSO or manually dissolved to 10mM in DMSO.

Manual organoid drug screening

384-well plates (Corning #3764) were coated with 8μl diluted BME (10mg/ml), followed by centrifugation at 250rpm for 1min at 4°C and kept overnight at 4°C. 20min before seeding of the organoids the coated plate was placed in the incubator at 37°C. Organoids from matrigel drops were washed with ice-cold PBS and the pellet was resuspended in TrypLE for 7min at 37°C to obtain single cells. Using a 10-100μl multichannel pipette 20μl/well organoid suspension and 10ul/well drug suspension were pipetted from a 96-well u-bottom plate to the coated 384-well plate. The plate was incubated for 6 days in an incubator. After 6 days the readout was performed using CellTiterGlo®3D reagent according to the manufacturer's protocol. Luminescence was measured by the BioTek plate reader Synergy H1 using Gen5 3.03. The raw luminescence data were normalized to [%] viability of negative control (0.1% DMSO) after identification and removal of outliers. All drug screening experiments have been performed in at least two biological and two technical replicates.

FDA-approved compound automated library screen

Organoids of the PC02 and PC02e lines were expanded using droplet cultures of Matrigel, covered with complete organoid medium as described above. Organoids were collected and dissociated to yield a single-cell suspension of $3.7*10^5$ cells per ml. Meanwhile, 384-well black tissue-culture plates (Corning #3764) were coated with 10μl cold gel coating mix (80%v/v Matrigel/ 20%v/v complete organoid medium) using a Tecan EVO 100 liquid handler (Tecan AG, Männedorf, Switzerland) integrated into a lab automation system (HighRes Biosolutions Ltd, Beverly MA, USA). After plate coating, plates were incubated for 30 minutes at 37°C in a SteriStore D incubator (HighRes Biosolutions Ltd, Beverly MA, USA). 27μl of PC02 or PC02e cells suspension in complete organoid medium (10'000c/well) w dispensed to each well of pre-coated 384-well plates using a BioTek EL406 with wide-bore tubing (BioTek, Winooski VT, USA), cleaned with 2% Bomix, 70% EtOH and sterilized MilliQ water. Subsequently, drugs of the FDA-approved drug library (L1300, Selleck Chemicals) were thawed and after dilution in basis medium, 3 μl per well were added resulting in a final concentration of 1μM, alongside positive controls gemcitabine and paclitaxel as well as solvent control (DMSO). After incubation for 6 days at 37°C in an atmosphere of 5% CO_2 at 95% humidity, 5μl CellTiterGlo®3D was added to all wells using a Tecan EVO 100. Plates were shaken for 15 minutes on a BioTek EL406 (BioTek, Winooski VT, USA), then incubated at room temperature for 15 minutes. Luminescence was measured using a Tecan M1000 Pro plate reader (Tecan AG, Männedorf, Switzerland) with 1000ms integration time to reflect the number of viable cells. All automated procedures were automated and scheduled with the software Cellario 3.2.

Analysis of automated screen results—Luminescence readout results obtained were exported and stored in spreadsheets and processed using a workflow implemented in the R environment for statistical computing [62,63] . This workflow was used to link luminescence results to the plate layout using plate tracking files generated with Cellario 3.2. Row- or

column wise stripe patterns or edge effects were corrected using the median polish method of Tukey. Systematic variation from plate to plate was removed by standard normalization procedures [64], and assay quality was evaluated on the basis of Z' factors [65]. Differential compound activity was assessed using a Z-test performed against the null hypothesis that the activity of the respective compound is indistinguishable from the negative controls. P-values were subsequently adjusted using the Benjamini & Hochberg method. Hits were subsequently selected according to FDR (<0.01) and effect size (0.5).

Drug screening in monolayer cultures

PANC-1 and ASPC-1 cell lines were a gift from the Wilhelm Krek Lab (ETH Zurich, Switzerland). PDAC monolayer cell lines were established by culturing organoid cell suspensions on cell culture plates. Cells were grown in the following media supplemented with 50 U/ml penicillin, 50 U/L of streptomycin and 10% fetal bovine serum: DMEM (PANC-1) and RPMI 1640 (ASPC-1, PDAC Organoid derived monolayer cell lines). For monolayer screening cells were trypsinized and counted using Countess I Cell Counter (Invitrogen) 1'000 cells per well were added to a 384-well plate with the corresponding compounds of interest. The plate was incubated for 72h and the readout performed using CellTiter-Glo®3D reagent according to the manufacturer's protocol. Luminescence was measured by the BioTek plate reader Synergy H1 using Gen5 3.03. The raw luminescence data were filtered for outliers and converted to viability in [%] by normalizing to the DMSO controls. All drug screening experiments have been performed in at least two biological and two technical replicates.

Compounds testing *in vivo*

Animal experiments were carried out at the Charles River Research Services Germany facility in Freiburg, Germany, and at the ETH Zurich phenomics center in accordance with the Declaration of Helsinki and international GV-SOLAs guidelines. All experiments were approved by the local ethics committee. Animal sample size per group was calculated based on previous studies (n=4-6). For organoid re-transplantation 3-6 drops of Matrigel corresponding to 100-500k cells were washed with ice cold Advanced DMEM and organoid pellet resuspend 1:1 in Matrigel before injection into 4-6 weeks old female NMRI nu/nu-mice. For pharmacological studies cells were transplanted in the flanks at Day 0 using a 1:1 dilution with Matrigel. When the tumor reached 100mm^3 animals were randomized to the different treatment groups and treatment applied according to predefined schedules (Table S7). The endpoint was defined as tumor volume exceeding 2'000mm^3 or signs of treatment toxicity monitored by weight and behavior. Mice were kept in the animal facility with 12h of light-dark cycle and with food and water *ad libitum*.

HIF-Reporter assay

A stable HIF luminescence PDAC reporter line was generated by using the previously established pLenti HRE-Luc pGK Hygro construct (Briggs KJ, Cell 2016) stable integrated into a PANC-1 cell line. Using a hypoxia chamber (1% O_2) effect on drug administration was assessed after 24h. Readout was performed using Promega Bright-Glo Reagent according to the manufacturer's instructions.

TCGA Survival Analysis

The 150 annotated PDAC samples of the TCGA-PAAD cohort have been used to generate the survival curve using the log2 mean expression of the 5 hypoxia genes (CAIX, SLC2A1, HK2, PKM, VEGFA).

Statistical analysis

Clustering was performed using an unsupervised clustering by Ward.D2 (Murtagh and Legendre 2014, Ward's clustering criterion). For correlation studies a Spearman rank correlation analysis was performed. Statistical comparisons between groups was performed using a 1 or 2-way ANOVA test with a Dunnett post-hoc-test. To compare groups of gene expression studies we used a pairwise Wilcoxon rank sum test corrected for multiple testing by Benjamini-Hochberg. In all cases, the significance level was set to $\alpha = 0.05$. P-values are indicated with *<0.05, **<0.01 and ***<0.001 or its numerical value.

Supplementary Material

Refer to Web version on PubMed Central for supplementary material.

Acknowledgements

Abbreviations

CNV	copy-number variant
PDAC	Pancreatic Ductal Adenocarcinoma
PDX	patient-derived xenografts
WT	Wildtype
SNV	single nucleotide variant
WES	whole exome sequencing
WGS	whole genome sequencing

Data and code availability

- PICNIC processed Affymetrix SNP6.0 data and processed WES data for the organoid lines established from PDX tumor tissue provided by Oncotest can

be freely accessed at the Charles River Tumor Model Compendium "https://compendium.criver.com" in the section pancreatic cancer (PAX). The Charles River nomenclature of the PDX lines used in this study is shown in Table S1. All raw sequencing files (WGS, WES and transcriptomics data) and raw Affymetrix SNP6.0 files that support the results presented in this paper are deposited in Sequence Read Archive (SRA) (accession numbers: PRJNA774495 and PRJNA800191) or Gene Expression Omnibus (GEO: GSE196183). Original western blot images have been deposited at figshare and are publicly available as of the date of publication. The DOI is listed in the key resources table. Microscopy data reported in this paper will be shared by the lead contact upon request.

- All scripts and codes used in this study are listed in the key resource table, and DOI or weblinks are provided.

- Any additional information required to reanalyze the data reported in this paper is available from the lead contact upon request.

References

1. Rawla P, Sunkara T, Gaduputi V. Epidemiology of Pancreatic Cancer: Global Trends, Etiology and Risk Factors. World J Oncol. 2019; 10: 10. [PubMed: 30834048]

2. Kamisawa T, Wood LD, Itoi T, Takaori K. Pancreatic cancer. Lancet. 2016; 388: 73–85. [PubMed: 26830752]

3. Oettle H, Neuhaus P, Hochhaus A, Hartmann JT, Gellert K, Ridwelski K, Niedergethmann M, Zülke C, Fahlke J, Arning MB, et al. Adjuvant chemotherapy with gemcitabine and long-term outcomes among patients with resected pancreatic cancer: The CONKO-001 randomized trial. JAMA - J Am Med Assoc. 2013; 310: 1473–1481.

4. Conroy T, Hammel P, Hebbar M, Ben Abdelghani M, Wei AC, Raoul JL, Choné L, Francois E, Artru P, Biagi JJ, et al. FOLFIRINOX or gemcitabine as adjuvant therapy for pancreatic cancer. New England Journal of Medicine, (Massachussetts Medical Society). 2018. 2395–2406.

5. Muranaka T, Kuwatani M, Komatsu Y, Sawada K, Nakatsumi H, Kawamoto Y, Yuki S, Kubota Y, Kubo K, Kawahata S, et al. Comparison of efficacy and toxicity of FOLFIRINOX and gemcitabine with nab-paclitaxel in unresectable pancreatic cancer. J Gastrointest Oncol. 2017; 8: 566–571. [PubMed: 28736643]

6. Conroy T, Desseigne F, Ychou M, Bouché O, Guimbaud R, Bécouarn Y, Adenis A, Raoul J-L, Gourgou-Bourgade S, de la Fouchardière C, et al. FOLFIRINOX versus Gemcitabine for Metastatic Pancreatic Cancer. N Engl J Med. 2011; 364: 1817–1825. [PubMed: 21561347]

7. Garrido-Laguna I, Hidalgo M. Pancreatic cancer: from state-of-the-art treatments to promising novel therapies. Nat Rev Clin Oncol. 2015; 12: 319–334. [PubMed: 25824606]

8. Gnanamony M, Gondi CS. Chemoresistance in pancreatic cancer: Emerging concepts. Oncol Lett. 2017; 13: 2507–2513. [PubMed: 28454427]

9. Moore MJ, Goldstein D, Hamm J, Figer A, Hecht JR, Gallinger S, Au HJ, Murawa P, Walde D, Wolff RA, et al. Erlotinib plus gemcitabine compared with gemcitabine alone in patients with advanced pancreatic cancer: A phase III trial of the National Cancer Institute of Canada Clinical Trials Group. J Clin Oncol. 2007; 25: 1960–1966. [PubMed: 17452677]

10. Sharma SV, Haber DA, Settleman J. Cell line-based platforms to evaluate the therapeutic efficacy of candidate anticancer agents. Nat Rev Cancer. 2010; 10: 241–253. [PubMed: 20300105]

11. Ling A, Gruener RF, Fessler J, Huang RS. More than fishing for a cure: The promises and pitfalls of high throughput cancer cell line screens. Pharmacol Ther. 2018; 191: 178–189. [PubMed: 29953899]

12. Bleijs M, Wetering M, Clevers H, Drost J. Xenograft and organoid model systems in cancer research. EMBO J. 2019; 38

13. Baker LA, Tiriac H, Clevers H, Tuveson DA. Modeling Pancreatic Cancer with Organoids. Trends in Cancer. 2016; 2: 176–190. [PubMed: 27135056]

14. Boj SF, Hwang C-I, Baker LA, Chio IIC, Engle DD, Corbo V, Jager M, Ponz-Sarvise M, Tiriac H, Spector MS, et al. Organoid Models of Human and Mouse Ductal Pancreatic Cancer. Cell. 2015; 160: 324–338. [PubMed: 25557080]

15. Seino T, Kawasaki S, Shimokawa M, Tamagawa H, Toshimitsu K, Fujii M, Ohta Y, Matano M, Nanki K, Kawasaki K, et al. Human Pancreatic Tumor Organoids Reveal Loss of Stem Cell Niche Factor Dependence during Disease Progression. Cell Stem Cell. 2018; 22: 454–467. e6 [PubMed: 29337182]

16. Tiriac H, Belleau P, Engle DD, Plenker D, Deschênes A, Somerville TDD, Froeling FEM, Burkhart RA, Denroche RE, Jang GH, et al. Organoid profiling identifies common responders to chemotherapy in pancreatic cancer. Cancer Discov. 2018; 8: 1112–1129. [PubMed: 29853643]

17. Vlachogiannis G, Hedayat S, Vatsiou A, Jamin Y, Fernández-Mateos J, Khan K, Lampis A, Eason K, Huntingford I, Burke R, et al. Patient-derived organoids model treatment response of metastatic gastrointestinal cancers. Science. 2018; 359: 920–926. [PubMed: 29472484]

18. Yao Y, Xu X, Yang L, Zhu J, Wan J, Shen L, Xia F, Fu G, Deng Y, Pan M, et al. Patient-Derived Organoids Predict Chemoradiation Responses of Locally Advanced Rectal Cancer. Cell Stem Cell. 2019.

19. Ooft SN, Weeber F, Dijkstra KK, McLean CM, Kaing S, van Werkhoven E, Schipper L, Hoes L, Vis DJ, van de Haar J, et al. Patient-derived organoids can predict response to chemotherapy in metastatic colorectal cancer patients. Sci Transl Med. 2019; 11

20. Driehuis E, van Hoeck A, Moore K, Kolders S, Francies HE, Gulersonmez MC, Stigter ECA, Burgering B, Geurts V, Gracanin A, et al. Pancreatic cancer organoids recapitulate disease and allow personalized drug screening. Proc Natl Acad Sci U S A. 2019.

21. Broutier L, Mastrogiovanni G, Verstegen MMA, Francies HE, Gavarró LM, Bradshaw CR, Allen GE, Arnes-Benito R, Sidorova O, Gaspersz MP, et al. Human primary liver cancer-derived organoid cultures for disease modeling and drug screening. Nat Med. 2017; 23: 1424–1435. [PubMed: 29131160]

22. Choi, SIl; Jeon, A-R; Kim, MK; Lee, Y-S; Im, JE; Koh, J-W; Han, S-S; Kong, S-Y; Yoon, K-A; Koh, Y-H; , et al. Development of Patient-Derived Preclinical Platform for Metastatic Pancreatic Cancer: PDOX and a Subsequent Organoid Model System Using Percutaneous Biopsy Samples. Front Oncol. 2019; 9

23. Lee SH, Hu W, Matulay JT, Silva MV, Owczarek TB, Kim K, Chua CW, Barlow LMJ, Kandoth C, Williams AB, et al. Tumor Evolution and Drug Response in Patient-Derived Organoid Models of Bladder Cancer. Cell. 2018; 73: 515–528. e17

24. Pauli C, Hopkins BD, Prandi D, Shaw R, Fedrizzi T, Sboner A, Sailer V, Augello M, Puca L, Rosati R, et al. Personalized in vitro and in vivo cancer models to guide precision medicine. Cancer Discov. 2017; 7: 462–477. [PubMed: 28331002]

25. Sachs N, de Ligt J, Kopper O, Gogola E, Bounova G, Weeber F, Balgobind AV, Wind K, Gracanin A, Begthel H, et al. A Living Biobank of Breast Cancer Organoids Captures Disease Heterogeneity. Cell. 2018; 172: 373–386. e10 [PubMed: 29224780]

26. Schütte M, Risch T, Abdavi-Azar N, Boehnke K, Schumacher D, Keil M, Yildiriman R, Jandrasits C, Borodina T, Amstislavskiy V, et al. Molecular dissection of colorectal cancer in pre-clinical models identifies biomarkers predicting sensitivity to EGFR inhibitors. Nat Commun. 2017; 8

27. Shi R, Radulovich N, Ng C, Liu N, Notsuda H, Cabanero M, N Martins-Filho S, Raghavan V, Li Q, Mer AS, et al. Organoid cultures as preclinical models of non-small cell lung cancer. Clin Cancer Res. 2019.

28. van de Wetering M, Francies HE, Francis JM, Bounova G, Iorio F, Pronk A, van Houdt W, van Gorp J, Taylor-Weiner A, Kester L, et al. Prospective derivation of a living organoid biobank of colorectal cancer patients. Cell. 2015; 161: 933–945. [PubMed: 25957691]

29. Shugang X, Hongfa Y, Jianpeng L, Xu Z, Jingqi F, Xiangxiang L, Wei L. Prognostic Value of SMAD4 in Pancreatic Cancer: A Meta-Analysis. Transl Oncol. 2016; 9: 1–7. [PubMed: 26947875]

30. Bailey P, Chang DK, Nones K, Johns AL, Patch AM, Gingras MC, Miller DK, Christ AN, Bruxner TJC, Quinn MC, et al. Genomic analyses identify molecular subtypes of pancreatic cancer. Nature. 2016; 531: 47–52. [PubMed: 26909576]

31. Biankin AV, Waddell N, Kassahn KS, Gingras M-C, Muthuswamy LB, Johns AL, Miller DK, Wilson PJ, Patch A-M, Wu J, et al. Pancreatic cancer genomes reveal aberrations in axon guidance pathway genes. Nature. 2012; 491: 399–405. [PubMed: 23103869]

32. Puleo F, Nicolle R, Blum Y, Cros J, Marisa L, Demetter P, Quertinmont E, Svrcek M, Elarouci N, Iovanna J, et al. Stratification of Pancreatic Ductal Adenocarcinomas Based on Tumor and Microenvironment Features. Gastroenterology. 2018; 155: 1999–2013. [PubMed: 30165049]

33. Waddell N, Pajic M, Patch A-M, Chang DK, Kassahn KS, Bailey P, Johns AL, Miller D, Nones K, Quek K, et al. Whole genomes redefine the mutational landscape of pancreatic cancer. Nature. 2015; 518: 495–501. [PubMed: 25719666]

34. Witkiewicz AK, McMillan EA, Balaji U, Baek G, Lin W-C, Mansour J, Mollaee M, Wagner K-U, Koduru P, Yopp A, et al. Whole-exome sequencing of pancreatic cancer defines genetic diversity and therapeutic targets. Nat Commun. 2015; 6: 6744. [PubMed: 25855536]

35. Fukumoto T, Magno E, Zhang R. SWI/SNF Complexes in Ovarian Cancer: Mechanistic Insights and Therapeutic Implications. Mol Cancer Res. 2018; 16: 1819–1825. [PubMed: 30037854]

36. Morel D, Almouzni G, Soria J-C, Postel-Vinay S. Targeting chromatin defects in selected solid tumors based on oncogene addiction, synthetic lethality and epigenetic antagonism. Ann Oncol Off J Eur Soc Med Oncol. 2017; 28: 254–269.

37. Helleday T. The underlying mechanism for the PARP and BRCA synthetic lethality: Clearing up the misunderstandings. Mol Oncol. 2011; 5: 387–393. [PubMed: 21821475]

38. Pilié PG, Gay CM, Byers LA, O'Connor MJ, Yap TA. PARP Inhibitors: Extending Benefit Beyond BRCA-Mutant Cancers. Clin Cancer Res. 2019; 25: 3759–3771. [PubMed: 30760478]

39. Sachdev E, Tabatabai R, Roy V, Rimel BJ, Mita MM. PARP Inhibition in Cancer: An Update on Clinical Development. Target Oncol. 2019.

40. Lai E, Ziranu P, Spanu D, Dubois M, Pretta A, Tolu S, Camera S, Liscia N, Mariani S, Persano M, et al. BRCA-mutant pancreatic ductal adenocarcinoma. Br J Cancer. 2021; 2021: 1–12.

41. Reiss KA, Yu S, Judy R, Symecko H, Nathanson KL, Domchek SM. Retrospective Survival Analysis of Patients With Advanced Pancreatic Ductal Adenocarcinoma and Germline BRCA or PALB2 Mutations. 2018.

42. Yosifov DY, Idler I, Bhattacharya N, Reichenzeller M, Close V, Ezerina D, Scheffold A, Jebaraj BMC, Kugler S, Bloehdorn J, et al. Oxidative stress as candidate therapeutic target to overcome microenvironmental protection of CLL. Leukemia. 2019.

43. Hoffmann AC, Mori R, Vallbohmer D, Brabender J, Klein E, Drebber U, Baldus SE, Cooc J, Azuma M, Metzger R, et al. High expression of HIF1a is a predictor of clinical outcome in patients with prancreatic ductal adenocarcinomas and correlated to PDGFA, VEGF, and bFGF. Neoplasia. 2008; 10: 674–679. [PubMed: 18592007]

44. Ehrenberg KR, Gao J, Oppel F, Frank S, Kang N, Dieter SM, Herbst F, Möhrmann L, Dubash TD, Schulz ER, et al. Systematic Generation of Patient-Derived Tumor Models in Pancreatic Cancer. Cells. 2019; 8: 142.

45. Krempley BD, Yu KH. Preclinical models of pancreatic ductal adenocarcinoma. Chinese Clin Oncol. 2017; 6: 3.

46. Yu K, Chen B, Aran D, Charalel J, Yau C, Wolf DM, van 'tVeer LJ, Butte AJ, Goldstein T, Sirota M. Comprehensive transcriptomic analysis of cell lines as models of primary tumors across 22 tumor types. Nat Commun. 2019; 10

47. Le Tourneau C, Delord J-P, Gonçalves A, Gavoille C, Dubot C, Isambert N, Campone M, Trédan O, Massiani M-A, Mauborgne C, et al. Molecularly targeted therapy based on tumour molecular profiling versus conventional therapy for advanced cancer (SHIVA): a multicentre, open-label, proof-of-concept, randomised, controlled phase 2 trial. Lancet Oncol. 2015; 16: 1324–1334. [PubMed: 26342236]

48. Kane RC, Cohen MH, Broder LE, Bull MI, Creaven PJ, Fossieck BE. Phase I-II evaluation of emetine (NSC-33669) in the treatment of epidermoid bronchogenic carcinoma. Cancer Chemother Reports. 1975; 59: 1171–1172.

49. Panettiere F, Coltman CA. Phase I experience with emetine hydrochloride (NSC 33669) as an antitumor agent. Cancer. 1971; 27: 835–841. [PubMed: 4929936]

50. Uzor PF. Recent developments on potential new applications of emetine as anti-cancer agent. EXCLI J. 2016; 15: 323–328. [PubMed: 27366142]

51. Foreman KE, Jesse JN, Kuo PC, Gupta GN. Emetine dihydrochloride: A novel therapy for bladder cancer. J Urol. 2014; 191: 502–509. [PubMed: 24045224]

52. Sun Q, Yogosawa S, Iizumi Y, Sakai T, Sowa Y. The alkaloid emetine sensitizes ovarian carcinoma cells to cisplatin through downregulation of bcl-xL. Int J Oncol. 2015; 46: 389–394. [PubMed: 25310746]

53. Nair A, Jacob S. A simple practice guide for dose conversion between animals and human. J Basic Clin Pharm. 2016; 7: 27–31. [PubMed: 27057123]

54. Khajah MA, Mathew PM, Luqmani YA. Na+/K+ ATPase activity promotes invasion of endocrine resistant breast cancer cells. PLoS One. 2018; 3

55. Gkountela S, Castro-Giner F, Szczerba BM, Vetter M, Landin J, Scherrer R, Krol I, Scheidmann MC, Beisel C, Stirnimann CU, et al. Circulating Tumor Cell Clustering Shapes DNA Methylation to Enable Metastasis Seeding. Cell. 2019; 176: 98–112. e14 [PubMed: 30633912]

56. Calderón-Montaño JM, Burgos-Morón E, Orta ML, Maldonado-Navas D, García-Domínguez I, López-Lázaro M. Evaluating the cancer therapeutic potential of cardiac glycosides. Biomed Res Int. 2014; 2014

57. Strobach H, Wirth KE, Rojsathaporn K. Absorption, metabolism and elimination of strophanthus glycosides in man. Naunyn Schmiedebergs Arch Pharmacol. 1986; 334: 496–500. [PubMed: 3821940]

58. Pei H, Li L, Fridley BL, Jenkins GD, Kalari KR, Lingle W, Petersen G, Lou Z, Wang L. FKBP51 Affects Cancer Cell Response to Chemotherapy by Negatively Regulating Akt. Cancer Cell. 2009; 16: 259–266. [PubMed: 19732725]

59. Peran I, Madhavan S, Byers SW, McCoy MD. Curation of the pancreatic ductal adenocarcinoma subset of the cancer genome atlas is essential for accurate conclusions about survival-related molecular mechanisms. Clin Cancer Res. 2018; 24: 3813–3819. [PubMed: 29739787]

60. Díaz-Gay M, Vila-Casadesús M, Franch-Expósito S, Hernández-Illán E, Lozano JJ, Castellví-Bel S. Mutational Signatures in Cancer (MuSiCa): a web application to implement mutational signatures analysis in cancer samples. BMC Bioinforma. 2018; 19: 1–16.

61. Blokzijl F, Janssen R, van Boxtel R, Cuppen E. MutationalPatterns: comprehensive genome-wide analysis of mutational processes. Genome Med. 2018; 10: 1–16. [PubMed: 29301565]

62. Huber W, Carey VJ, Gentleman R, Anders S, Carlson M, Carvalho BS, Bravo HC, Davis S, Gatto L, Girke T, et al. Orchestrating high-throughput genomic analysis with Bioconductor. Nat Methods. 2015; 12: 115–121. [PubMed: 25633503]

63. Prummer M. Hypothesis testing in high-throughput screening for drug discovery. J Biomol Screen. 2012; 17: 519–529. [PubMed: 22233646]

64. Malo N, Hanley JA, Cerquozzi S, Pelletier J, Nadon R. Statistical practice in high-throughput screening data analysis. Nat Biotechnol. 2006; 24: 167–175. [PubMed: 16465162]

65. Zhang J-H, Chung, Oldenburg. A Simple Statistical Parameter for Use in Evaluation and Validation of High Throughput Screening Assays. J Biomol Screen. 1999; 4: 67–73. [PubMed: 10838414]
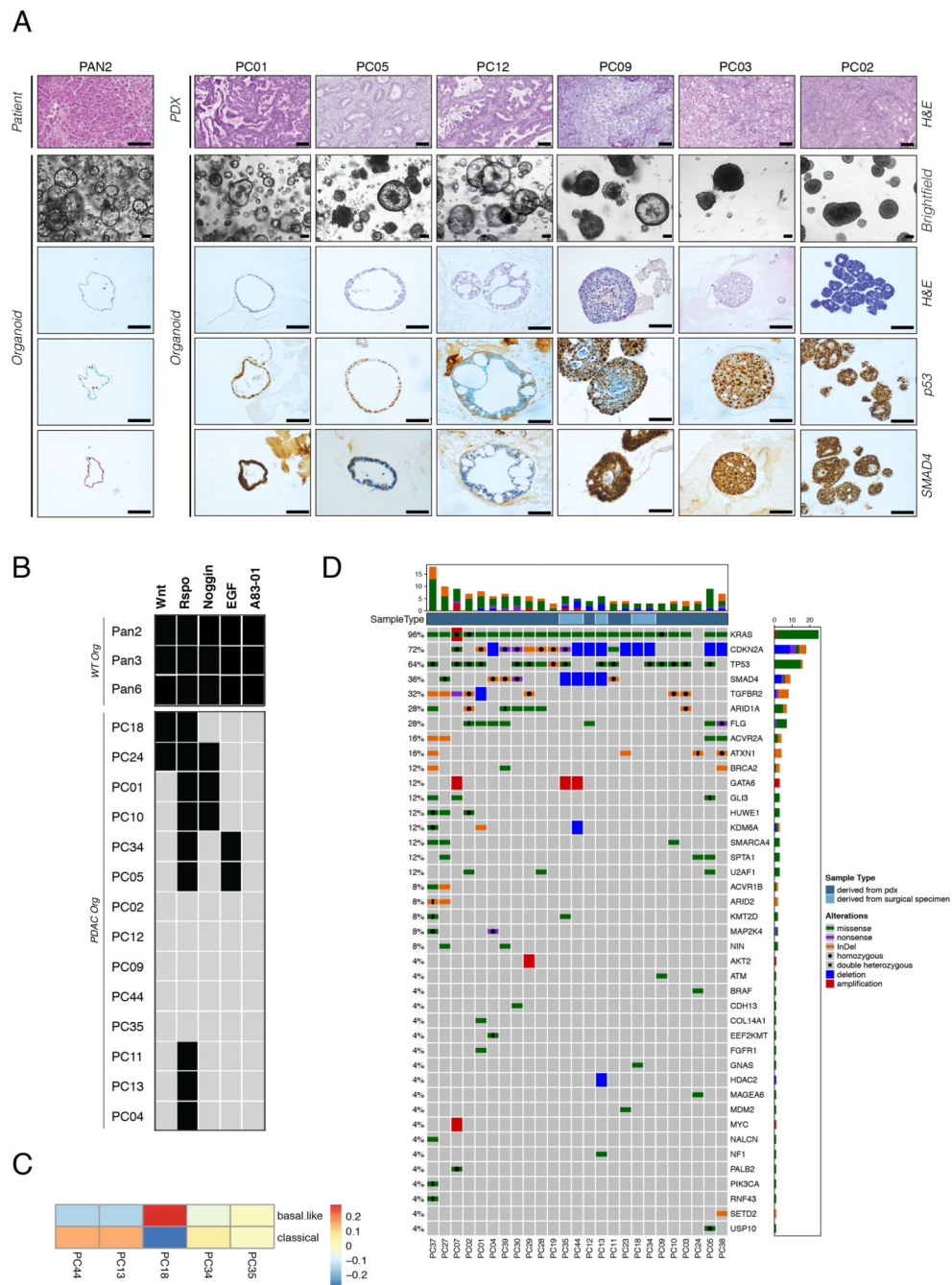
Figure 1. Phenotypic and molecular landscape of a PDAC organoid biobank

(A) Brightfield images and corresponding H&E-, p53- and SMAD4- stainings for one WT pancreas organoid line and several PDAC organoid lines. Corresponding *in vivo* phenotype is shown from patient or PDX tissue. Scale bar 100μm. (B) Growth factor dependencies of different PDAC and WT organoid lines after *in vitro* culture for 6 passages in growth factor depleted medium. Black box = growth factor dependent, gray box = growth factor independent. (C) Classification of PDAC organoids into either a basal-like or classical subtype based on RNA-seq profiles (Spearman correlation) using classification system by

Puleo et al. 2018 [32] . (D) Overview of mutations in PDAC driver genes observed in PDAC organoid lines of our biobank (see Table S2 for a full list of PDAC driver genes). PDAC organoids derived from surgical specimens are shown in brown, those derived from PDX-cell suspensions are shown in violet. The following mutations are indicated: SNVs (green), InDels (violet), amplifications (red), deletions (blue). The bar plots on the top depict the number of alterations in each sample, and the bar plots on the right depict the alteration frequencies for each gene in the biobank. See also Figure S1, and Tables S1-5.
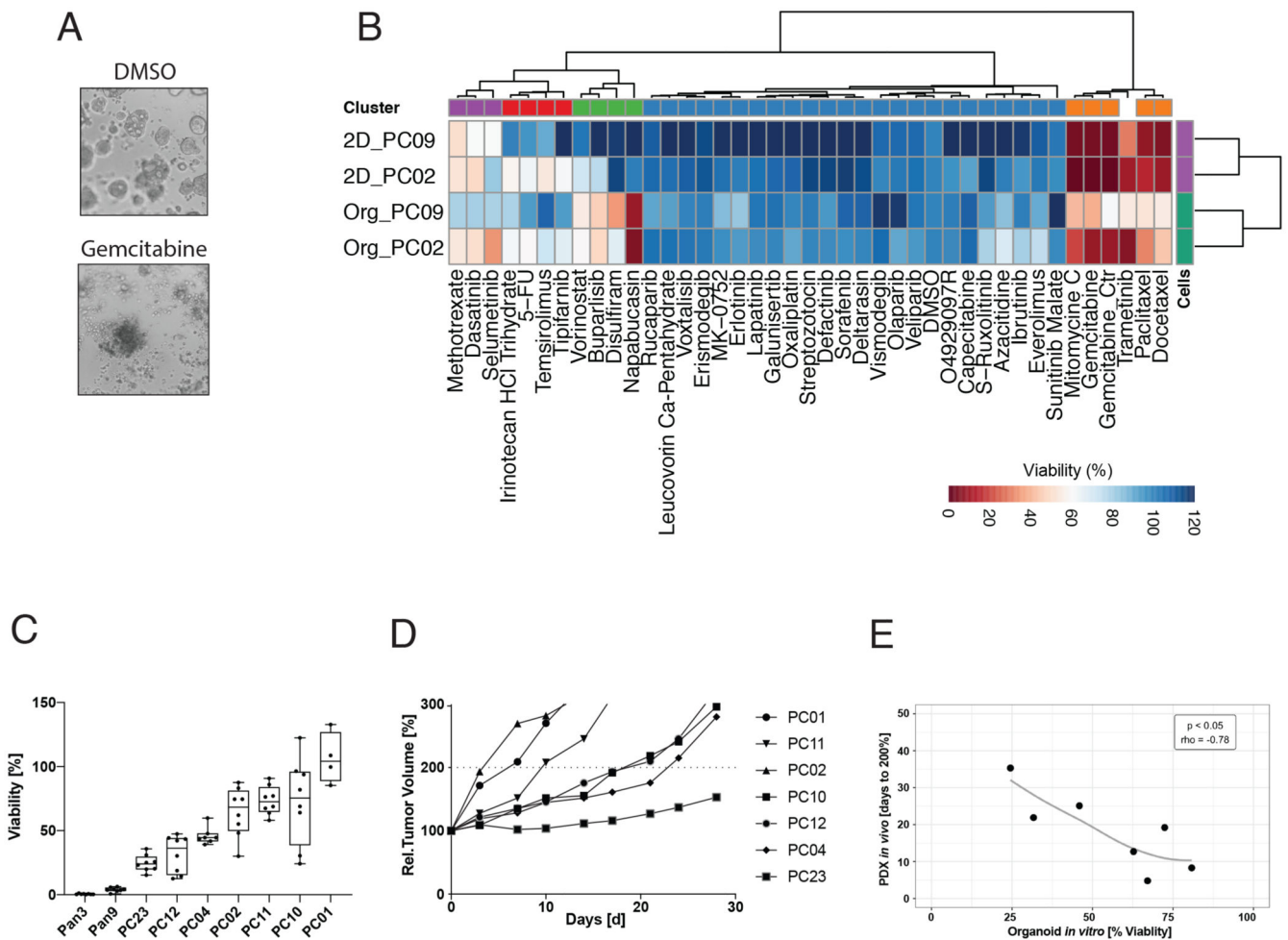
Figure 2. Drug response in PDAC organoids and PDX models are correlated

(A) Brightfield images for the PC02 PDAC organoid line, treated with DMSO control (upper panel) and the standard PDAC drug gemcitabine (1μM) (lower panel). (B) Drug response profile of paired isogenic PDAC organoid lines and corresponding monolayer cell lines (PC02 and PC09). Tested drugs are either approved for PDAC by the FDA or currently in clinical trials. Viability was normalized to solvent control (0.1% DMSO) and at a reference dose of 1μM (red = high sensitivity, blue = low sensitivity). Data displayed are averages of the technical and biological replicates. (C) Relative viability (compared to DMSO control) of WT pancreas organoid lines and PDAC organoid lines treated with 10 μM erlotinib. Technical replicates of two independent experiments are shown as Tukey plots. (D) Mean relative tumor volume of the same PDAC lines as shown in (c) grown as PDX models and treated with erlotinib (d=day, n=5 mice per group). (E) Correlation of drug responses for erlotinib *in vitro* (% viability at a dose of 10μM) and *in vivo* (Days to reach 200% tumor volume) using a Spearman's rank correlation test. See also Figure S2.
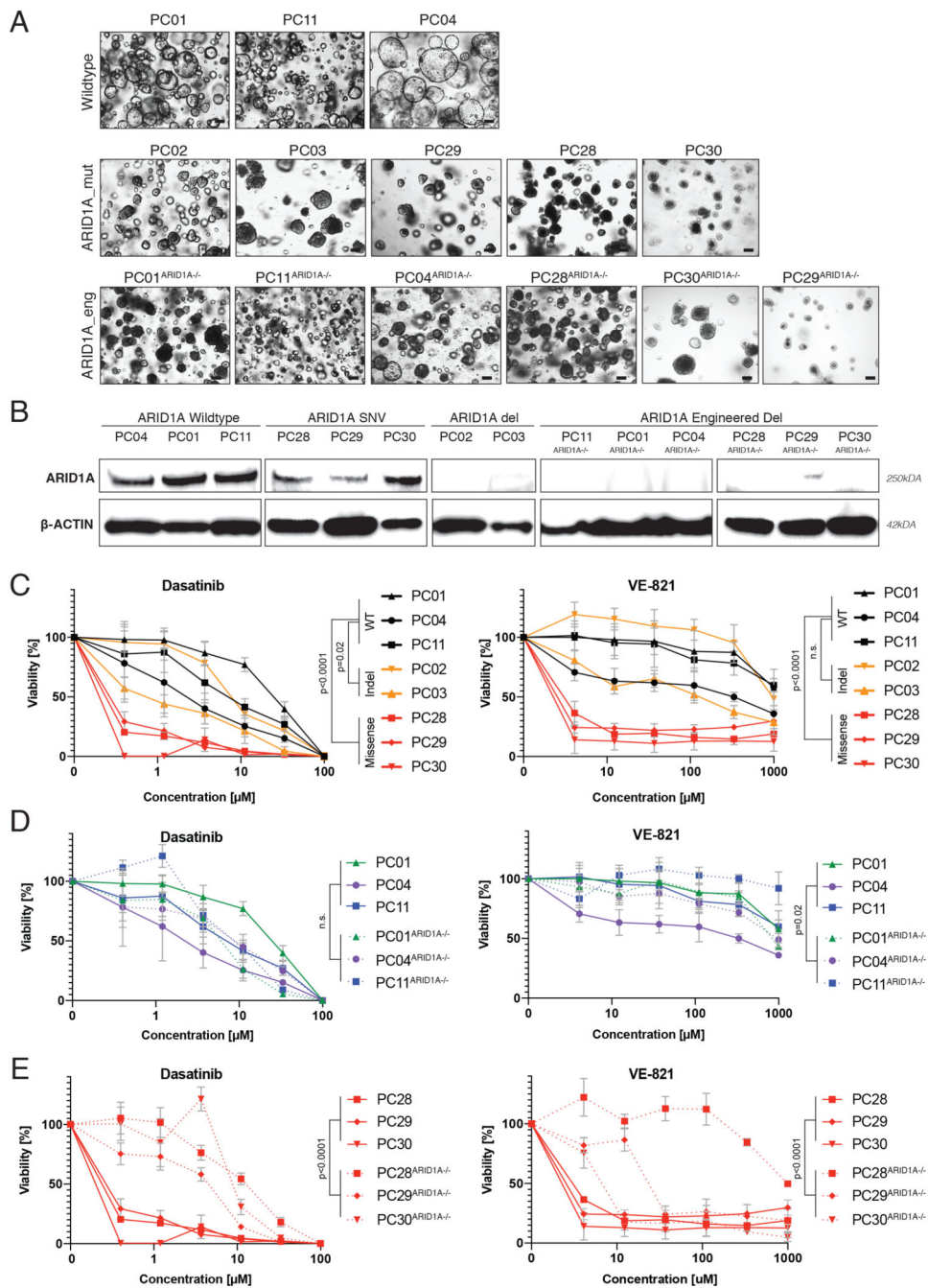
Figure 3. Assessment of *ARID1A* drug-gene interactions in PDAC organoids

(A) Phenotypes of PDAC organoids WT for *ARID1A* (top panel), mutant for *ARID1A* (middle panel), and engineered by CRISPR/Cas9 to become mutant for *ARID1A* (bottom panel). While *ARID1A* mutations in PC28 and in PC30 are recurrent tumor driver mutations (cBioPortal database), the mutation in PC29 has not yet been reported in pan-cancer or PDAC studies (cBioPortal database), or as a SNP in healthy populations (dbSNP, NCBI database). Scale bar 100μm. (B) Western blot showing ARID1A and β-ACTIN expression. (C) Response profile of genuine *ARID1A*-mutant organoids (yellow, red) and *ARID1A*-

WT organoids (black) to dasatinib (left panel) and VE-821 (right panel). Viability was normalized to solvent control (0.1% DMSO). Data is represented as means +/- SDs based on technical and biological replicates. (D) Response profile of *ARID1A*-WT organoids (full lines) and CRISPR-Cas9 engineered *ARID1A*-mutant organoids (dashed lines) to dasatinib (left panel) and VE-821 (right panel). Viability was normalized to solvent control (0.1% DMSO). Data plotted for *ARID1A*-WT organoids was derived from the same experiment as shown in C. Data is represented as means +/- SDs based on technical and biological replicates. (E) Effect of introducing an *ARID1A* frameshift mutation in three organoid lines that initially contained a missense mutation on dasatinib (left panel) and VE-821 (right panel) treatment. Viability was calculated by normalizing each dose to the DMSO treated control. Data plotted for *ARID1A*-missense organoids was derived from the same experiment as shown in C. Data is represented as means +/- SDs based on technical and biological replicates. See also Figure S3. Two-way ANOVA was used to compute the indicated p-values comparing the drug-response of the indicated samples.
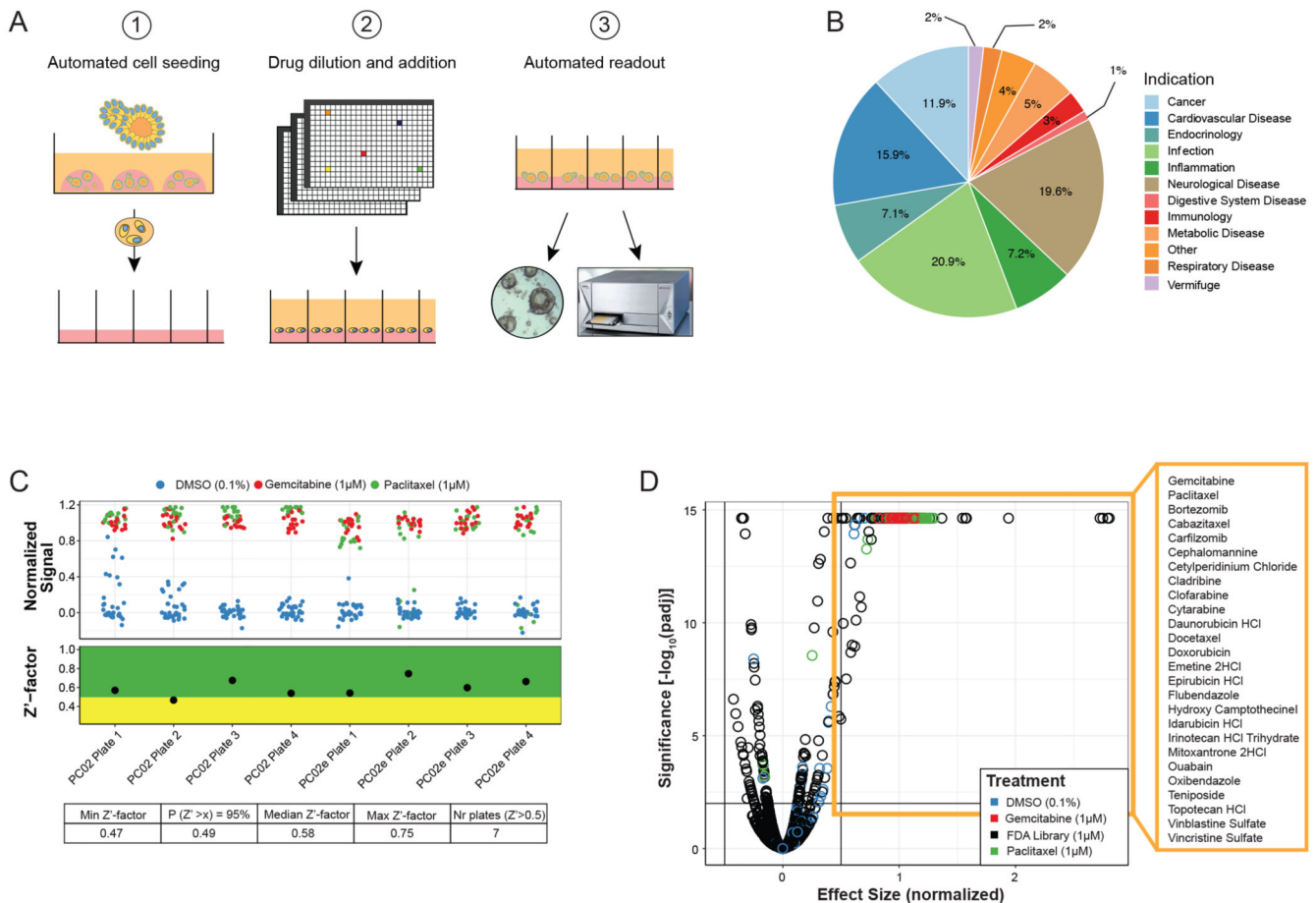
Figure 4. High-throughput drug screening in PDAC organoids
(A) Illustration of the fully automated screening pipeline which enables hydrogel coating, organoid cell seeding, drug delivery, and readout of the assay in a 384-well format. (B) Library composition of the 1,172 FDA-approved compounds with respect to indication. (C) Normalized signal of positive and negative controls (top) together with the visualization of the Z'-factors for each assay plate (center), and summarized statistics (bottom). (D) Volcano plot with identified hits highlighted. The horizontal line corresponds to FDR=0.01 and the two vertical lines represent a change of viability of 0.5. Hits were selected to have an FDR<0.01 and effect size >0.5. See also Figure S4 and Table S6.
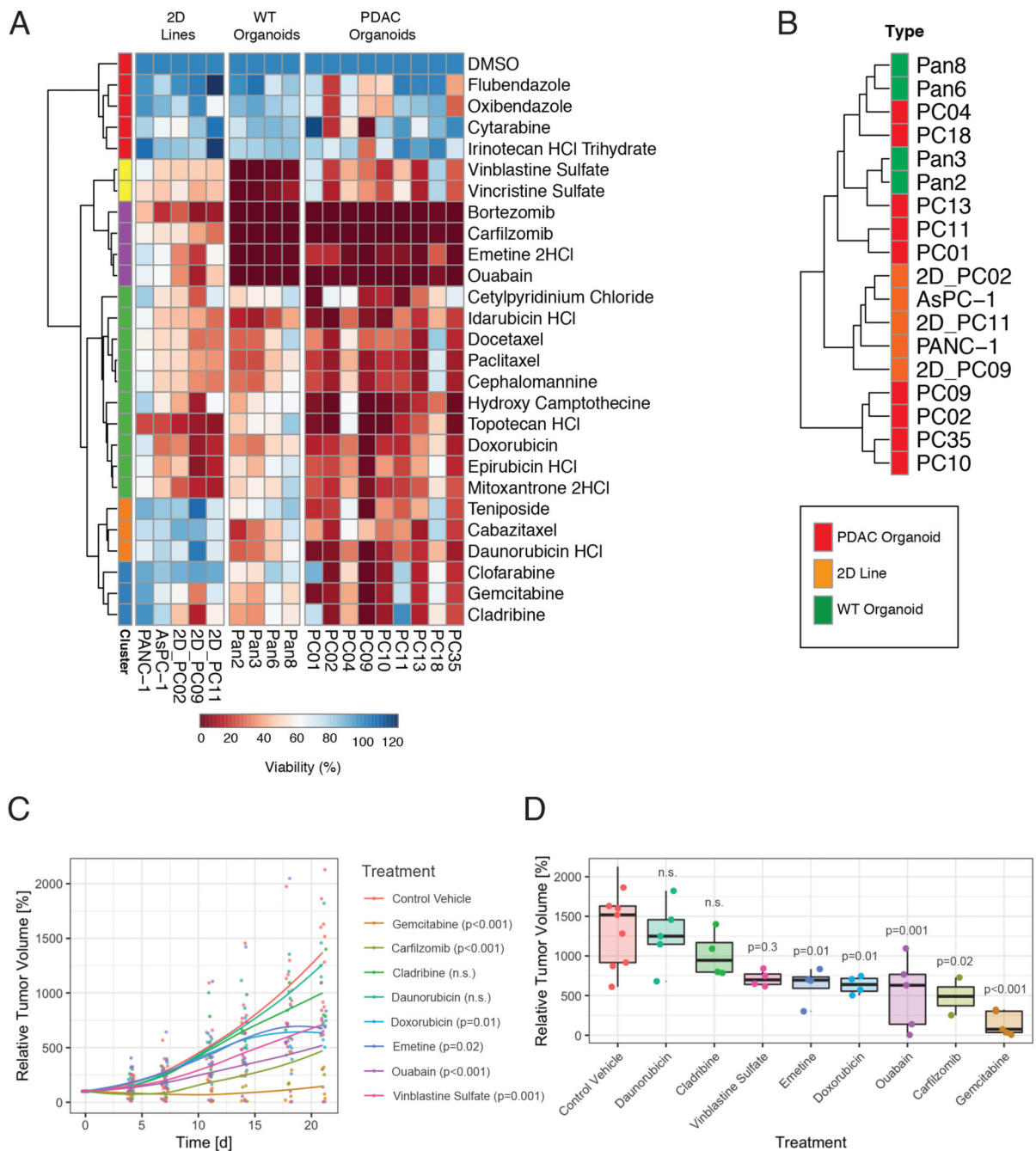
Figure 5. *In vitro* and *in vivo* validation of screening hits

(A) Heatmap indicating drug response of commercially available 2D PDAC cell lines, PDAC organoid-derived monolayer lines, WT pancreas organoids, and PDAC organoids. Colors from red to blue represent normalized [%] viability compared to solvent (0.1% DMSO) control. Viability was screened at a dose of 1μM (red = high sensitivity, blue = low sensitivity). Data is represented as averages based on technical and biological replicates. (B) Unsupervised clustering of different lines according to their drug response profile (green: WT pancreas organoid lines; red: PDAC organoid lines; orange: 2D PDAC cell lines). (C)

Growth curves represent the increase of relative tumor over the course of 21 days using the PC02-PDX model (n = 4-5 mice per group). The indicated statistical significance was computed using two-way ANOVA with Dunnett post-hoc test. (D) Relative tumor volume end of treatment period for the different groups. Data points represent individual mice used in the experiment. The indicated statistical significance was computed using one-way ANOVA with Dunnett post-hoc test. See also Figures S5 and S6 and Table S7.
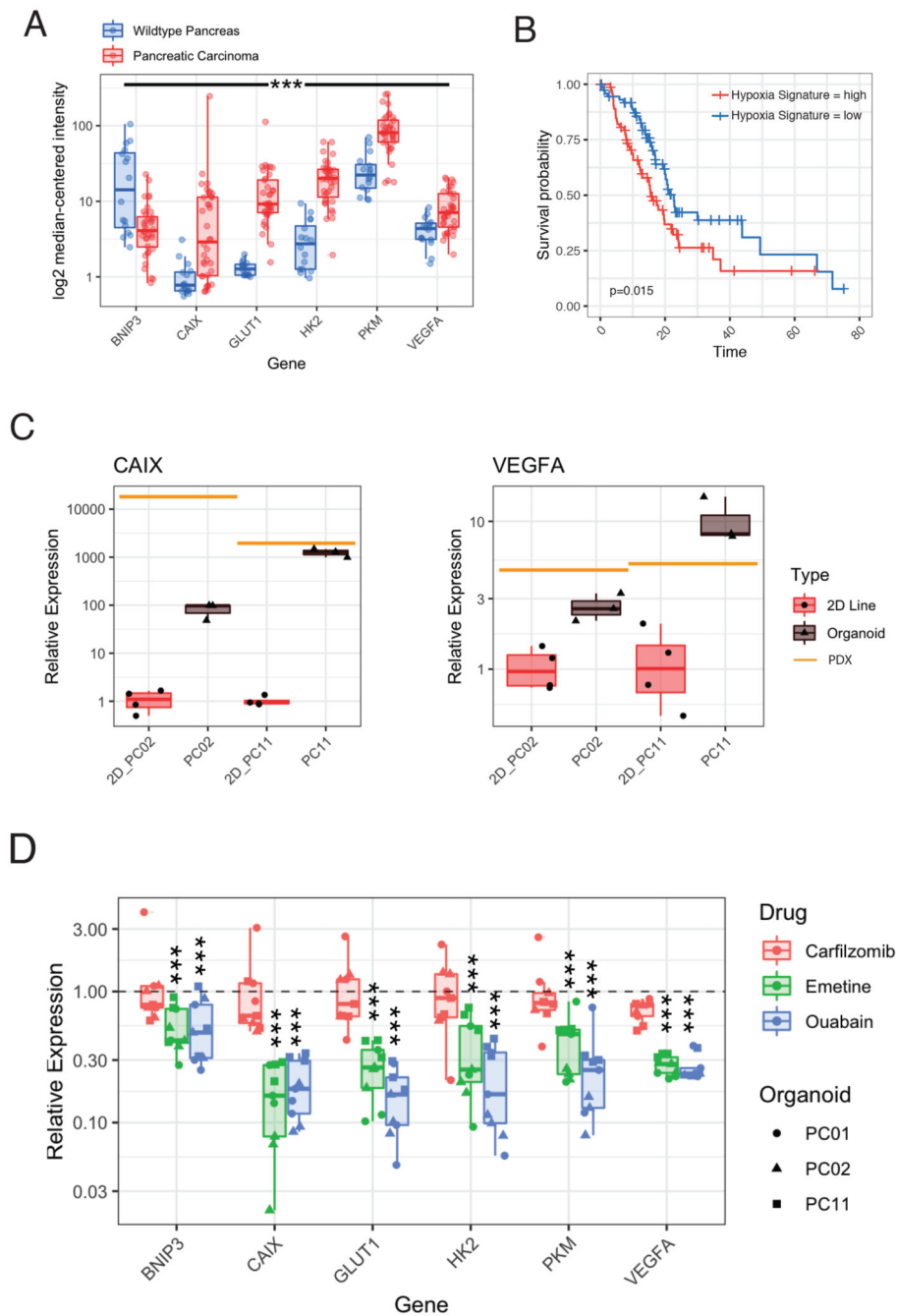
Figure 6. Ouabain and emetine suppress PDAC organoid growth by targeting the HIF response
(A) Log2 median-centered intensity of HIF-1α target gene expression in WT pancreas and PDAC patient tissue (Oncomine Microarray-Data Analysis from GEO GSE16515) [58]. ***<0.001; Pairwise Wilcoxon rank sum test with multiple testing corrected using Benjamini-Hochberg. (B) Correlation between PDAC patient survival and the hypoxia gene expression signature based on the log2 mean expression of 5 hypoxia response genes (CAIX, SLC2A1, HK2, PKM, VEGFA), red = low expression, blue = high expression). Misclassified samples of the TCGA-PAAD cohort were excluded and only the 150 correctly

classified PDAC samples were included in the analysis [59] . (C) *CAIX* and *VEGFA* expression relative to the housekeeping gene *TBP* measured by qPCR. Isogenic PDAC lines were grown as monolayer cultures (n=4), organoid cultures (n=3), or PDX models (n=1). (D) HIF-1α target gene expression by qPCR in 3 different human patient organoid lines 24h after emetine, ouabain or carfilzomib treatment relative to the solvent control group (DMSO 0.1%). 3 biological replicates are shown per individual patient organoid line. ***<0.001; Wilcoxon signed rank test with multiple testing corrected using Benjamini-Hochberg. See also Figure S7.